

Self-straining of actively crosslinked microtubule networks

Sebastian Fürthauer^{1*}, Bezia Lemma^{2,3,4}, Peter J. Foster⁵, Stephanie C. Ems-McClung⁶, Che-Hang Yu⁷, Claire E. Walczak⁶, Zvonimir Dogic^{3,4}, Daniel J. Needleman⁸ and Michael J. Shelley^{1,9}

Cytoskeletal networks are foundational examples of active matter and central to self-organized structures in the cell. In vivo, these networks are active and densely crosslinked. Relating their large-scale dynamics to the properties of their constituents remains an unsolved problem. Here, we study an in vitro active gel made from aligned microtubules and XCTK2 kinesin motors. Using photobleaching, we demonstrate that the gel's aligned microtubules, driven by motors, continually slide past each other at a speed independent of the local microtubule polarity and motor concentration. This phenomenon is also observed, and remains unexplained, in spindles. We derive a general framework for coarse graining microtubule gels crosslinked by molecular motors from microscopic considerations. Using microtubule–microtubule coupling through a force–velocity relationship for kinesin, this theory naturally explains the experimental results: motors generate an active strain rate in regions of changing polarity, which allows microtubules of opposite polarities to slide past each other without stressing the material.

Active materials are made from energy-consuming constituents whose activity keeps the system out of equilibrium. Their study has deepened our understanding of self-organizing processes, both in vivo and in vitro^{1,2}. Its foundational examples include suspensions of microswimmers, in vitro assemblies of purified cellular components and the cell cytoskeleton³. Although notable progress has been made in deciphering the non-equilibrium physics of active materials by using experiments and symmetry-based phenomenological theories^{4–6}, there is far less understanding of how the large-scale dynamics actually devolves from microscopic activity. Such a theoretical framework would allow for rational design of new active materials and quantitative understanding of the cell cytoskeleton. We address this challenge for systems made of cytoskeletal polymers that are fully percolated by moving molecular motors. First, we describe the microscopic dynamics of a dense nematic aligned active gel made from purified microtubules and XCTK2 kinesin motors. Using photobleaching and second harmonic generation (SHG) microscopy, we show that the microtubule sliding speeds are independent of the local gel polarity and motor concentration, suggesting a robust internal coupling of the filamentous material. To investigate this phenomenon, we introduce a framework for systematically deriving continuum theories of densely crosslinked active gels from prescribed microscopic considerations. We use this framework to obtain a theory for the XCTK2–microtubule system, which explains our experimental findings without adjustable parameters.

Many aspects of cell biology, including cell shape, motility and division, are driven by the cytoskeleton⁷. The cytoskeleton consists of polar filaments (mainly actin and microtubules) and the proteins that crosslink them and organize their behaviour. Molecular motors are active crosslinkers that use chemical energy to move filaments

relative to each other. They play a central role in determining the architecture and dynamics of cytoskeletal structures such as the cell cortex and the spindle³. How large-scale behaviours of actively crosslinked networks emerge from the properties of their constituents is important for quantitative understanding of the cellular cytoskeleton^{8–10}. The in vitro XCTK2–microtubule system that we study recapitulates the previously unexplained polarity-independent sliding motion of microtubules that was observed using speckle microscopy in *Xenopus* meiotic spindles^{11–13} and allows us to study how polarity-independent filament motion can emerge in actively crosslinked networks.

Phenomenological theories for actively crosslinked networks have been derived from conservation laws and symmetry considerations^{1,4–6,14}. They can reproduce the flow patterns observed in artificial¹⁵ and biological systems, such as the cell cortex^{8,16–18}, and quantitatively explain some aspects of spindle structure and dynamics¹⁹. However, such theories do not address how the large-scale behaviours of actively crosslinked networks emerge from the properties of their constituents. For this, an approach that derives macroscopic material laws from the properties of motors and filaments is needed.

Previous efforts to derive continuum theories for active gels from microscopic interactions have considered sparsely crosslinked systems, in which individual motor–filament clusters are thought of as disconnected objects^{20–30}. In contrast, actively crosslinked networks, such as the cytoskeleton³, are tightly coupled over length scales comparable to the system size and display behaviours different from those predicted for sparsely crosslinked active fluids. The rheological properties of highly crosslinked gels have been studied using combinations of numerical and analytical techniques^{31–35}. Here, we present an analytic framework for deriving continuum equations that capture their dynamics.

¹Center for Computational Biology, Flatiron Institute, New York, NY, USA. ²Department of Physics, Harvard University, Cambridge, MA, USA. ³Department of Physics, Brandeis University, Waltham, MA, USA. ⁴Department of Physics, University of California, Santa Barbara, CA, USA. ⁵Physics of Living Systems, Department of Physics, Massachusetts Institute of Technology, Cambridge, MA, USA. ⁶Medical Sciences, Indiana University, Bloomington, IN, USA.

⁷Department of Electrical and Computer Engineering, University of California, Santa Barbara, CA, USA. ⁸Paulson School of Engineering & Applied Science and Department of Molecular & Cellular Biology, Harvard University, Cambridge, MA, USA. ⁹Courant Institute, New York University, New York, NY, USA.

*e-mail: sfuertbauer@flatironinstitute.org

Experiments

To study the behaviour of heavily crosslinked active gels, we created one from purified microtubules and $0.4\ \mu\text{M}$ of XCTK2, a minus-end directed kinesin-14 molecular motor capable of crosslinking and sliding aligned microtubules³⁶. Fluorescently labelled tubulin and fluorescently labelled XCTK2 were mixed together, and then paclitaxel was added, which nucleated and stabilized the microtubules. The sample was rapidly loaded into a $0.1 \times 1 \times 20\ \text{mm}^3$ rectangular microfluidic chamber (see Supplementary Information). The microtubule–motor mixture contracted within the first ~ 10 min and formed a macroscopic gel, with its microtubules nematically aligned parallel to the long axis of the microfluidic chamber. The sample remained in this macroscopically aligned state for ~ 1 h, after which the gel buckled and displayed complex dynamics for hours longer. In this study, we characterize the motions of microtubules in the macroscopically aligned state of the gel, before buckling occurred.

We used a femtosecond laser to photobleach microtubules in the aligned gels, near the centre of the chamber, and investigate their dynamics. We generated multiple bleach lines orthogonal to the nematic director (Fig. 1a). Each of the bleached lines split into two parallel lines, which moved apart along the direction of alignment (Fig. 1b, left), indicating that microtubules in the gel are continually sliding relative to each other. Control experiments confirmed that the laser bleached, but did not ablate, the microtubules (see Supplementary Information).

When a bleached line splits into two, the relative fluorescent intensity of the two new lines reflects the relative number of left-moving and right-moving microtubules. Hence, the relative bleach intensity provides a measure of the polarity at the initial location of the bleach. We define the bleach polarity, $P_{\text{bleach}} = \left| \frac{I_1 - I_2}{I_1 + I_2} \right|$, where I_1 and I_2 are the bleach intensities of the two lines (see Supplementary Information). The speed at which the two lines move apart provides a measure of the speed of microtubule sliding. Along the same bleach line, some regions have very high polarity (Fig. 1b, orange, $P_{\text{bleach}} = 0.63 \pm 0.12$), while others have very low polarity (Fig. 1b, blue, $P_{\text{bleach}} = 0.08 \pm 0.17$). Despite this difference in polarity, the speed of sliding is very similar (Fig. 1b, right, compare orange and blue). We next performed experiments with varying motor concentrations. We measured the polarity and sliding speeds for four different motor concentrations (0.3, 0.4, 0.5 and $0.75\ \mu\text{M}$), each at many different locations, and found that the speed of microtubule sliding was independent of both polarity and motor concentration (Fig. 2). For motor concentrations below $0.3\ \mu\text{M}$, the microtubules did not contract and did not spontaneously align. For motor concentrations above $0.75\ \mu\text{M}$ the gels buckled before settling down into an aligned state. The average speed that microtubules slid apart in these XCTK2 active gels was $18.6 \pm 0.9\ \text{nm s}^{-1}$, which is very close to the observed speed of $20\ \text{nm s}^{-1}$ at which XCTK2 slides apart isolated pairs of microtubules³⁶.

P_{bleach} provides a local measure of the polarity of microtubule motion, that is, of the relative number of left-moving and right-moving microtubules. We next sought to determine to what extent this polarity of microtubule motion is related to the physical polarity of microtubules in the gel, that is, of the relative number of left-facing and right-facing microtubules. The physical polarity of microtubule arrays can be measured by simultaneous SHG, a non-linear optical technique in which a signal can be produced from non-centrosymmetric materials, and two-photon microscopy of fluorescent microtubules. The local physical polarity is proportional to $P_{\text{SHG}} = \sqrt{I_{\text{SHG}}/I_p^2}$, where I_{SHG} is the intensity measure from SHG and I_p is the intensity measure from two-photon microscopy³⁷. We simultaneously measured P_{SHG} and P_{bleach} at multiple locations, and found that they are highly correlated (Fig. 2, inset). Therefore, in

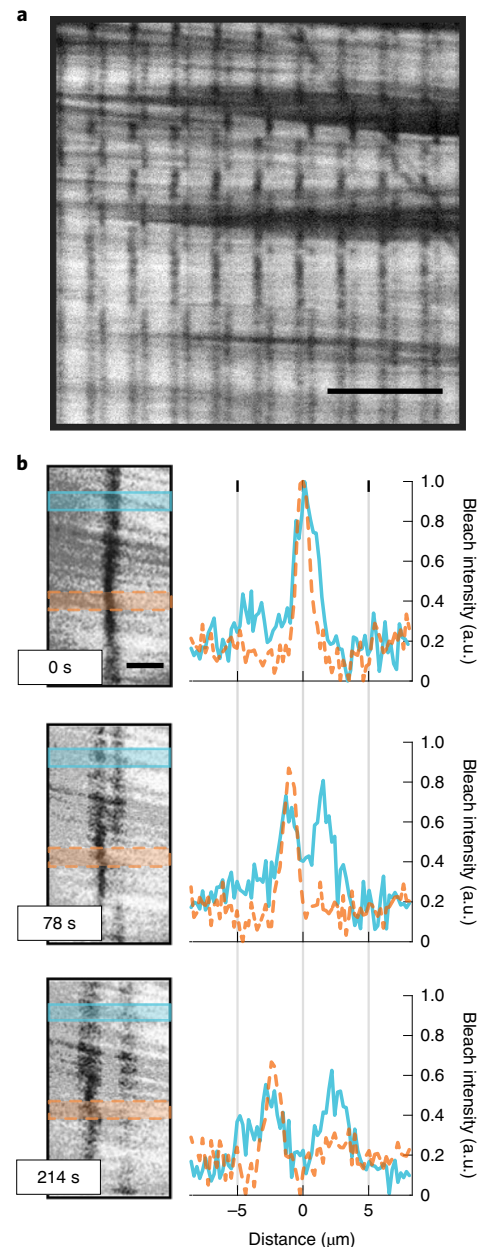


Fig. 1 | Bleaching of aligned active gels reveals microtubule sliding speed.

a, Aligned active gel after multi-line photobleaching. Scale bar, $20\ \mu\text{m}$. **b**, Left: higher magnification images of a bleached line taken at three different times. The bleached line with spatially varying polarity splits into two parallel lines as the microtubules slide apart. Solid blue and dashed orange shaded areas highlight regions of low and high polarity respectively. Right: intensity profiles of the high polarity (dashed orange, $P_{\text{bleach}} = 0.63 \pm 0.12$ standard error) and low polarity (solid blue, $P_{\text{bleach}} = 0.08 \pm 0.17$ standard error) regions. Despite the difference in polarity, the peaks move apart at nearly identical speeds. Scale bar, $5\ \mu\text{m}$. XCTK2 concentration is $0.4\ \mu\text{M}$.

this gel, the local dynamic polarity of microtubule motion reflects the local physical polarity of microtubules, and the microtubule sliding speed is independent of the local polarity. This is reminiscent of the independence of microtubule sliding speed and polarity observed in spindles^{11–13}.

The polarity-independent sliding speed of microtubules is difficult to reconcile with existing kinetic theories, which apply in the

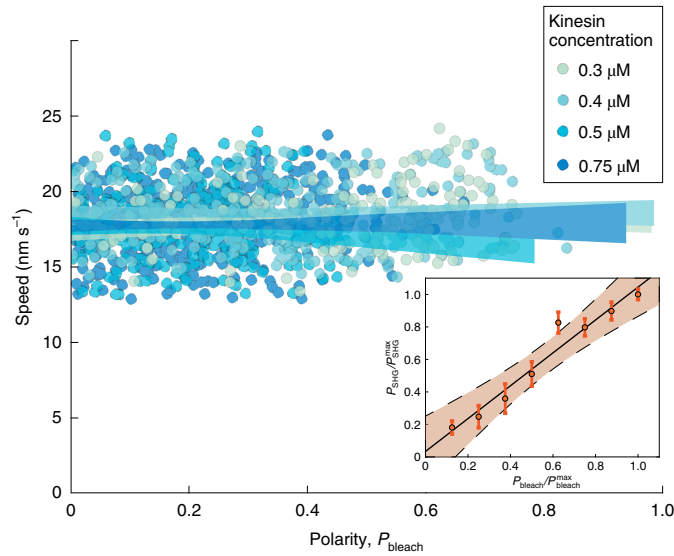


Fig. 2 | Microtubule sliding speed is independent of polarity and motor concentration. Local measurements (2 μm bins) from photobleaching of microtubule sliding speed and polarity, P_{bleach} , for different XCTK2 concentrations. The shaded regions indicate the 95% confidence intervals of a linear regression for each motor concentration. Inset: correlation between local polarity P_{bleach} of microtubule motion measured by bleaching and local physical polarity P_{SHG} of microtubules measured by SHG. The black line is a linear regression and the shaded region indicates the corresponding 99% confidence interval.

limit of dilute and sparsely crosslinked networks where the length scale over which filaments are interconnected is small compared to the system size. To illustrate the issue we describe previously presented arguments^{20,28}. In the absence of external driving forces, the balance of forces yields $\rho^+f^+ + \rho^-f^- = 0$, where ρ^\pm are the densities of microtubules pointing along the nematic axis of the system in the positive and negative directions, respectively, and f^\pm are the forces acting on microtubules from their interactions with \mp microtubules, respectively. In a sparsely crosslinked system the force exerted by a motor on a microtubule is balanced only by the drag between the microtubule and the surrounding medium. Assuming that the medium is locally at rest, the velocity of microtubules, v^\pm , will be given by $v^\pm = \mu f^\pm$, where μ is the microtubule mobility. A molecular motor crosslinking two microtubules moving at a speed V imposes $v^+ - v^- = 2V$. Taken together, this leads to $v^\pm = \mp V(1 \mp P)$, where $P = \frac{\rho^+ - \rho^-}{\rho^+ + \rho^-}$ is the local microtubule polarity.

The argument described above predicts that the microtubule sliding velocity changes linearly with polarity, in conflict with our experimental measurements of reconstituted gels and spindle. Fundamentally, this prediction is a consequence of force balance in sparsely crosslinked systems: the mass fluxes of left moving and right moving microtubules locally balance because the momentum transfer in the system is dominated by fluid-mediated interactions. Polarity-dependent sliding generalizes to more sophisticated versions of dilute theories that include effects such as long-range hydrodynamics (see Supplementary Information). The disagreement between this theory and experiment suggests that microtubule–XCTK2 gels may not be in a sparsely crosslinked regime. To examine this possibility, we quantified the microtubule density in our gel by measuring the initial molarity of components in our mixture and then determined the percentage of components that were incorporated into the final gel via fluorescence microscopy. We estimate a 5% volume fraction of polymerized microtubules in the gels, with 17 microtubules per μm^3 (see Supplementary Information)

and ~ 25 XCTK2 dimers bound to each microtubule. Given that microtubules are significantly longer than their average spacing, this result argues that these networks are heavily crosslinked by molecular motors—far from the dilute theory described above. Motivated by such considerations, we developed a model of heavily crosslinked microtubule networks.

Theory for densely crosslinked microtubule gels

In our theory, microtubules are characterized by their length L , velocities \mathbf{v}_i and orientations \mathbf{p}_i . The distribution of microtubule positions and orientations $\psi(\mathbf{x}, \mathbf{p}) = \sum_i \delta(\mathbf{x} - \mathbf{x}_i)\delta(\mathbf{p} - \mathbf{p}_i)$ obeys the Smoluchowski equation $\partial_t \psi = -\nabla \cdot (\dot{\mathbf{x}}\psi) - \partial_{\mathbf{p}} \cdot (\dot{\mathbf{p}}\psi)$. The microtubules’ translational and rotational fluxes, $\dot{\mathbf{x}}(\mathbf{x}_i, \mathbf{p}_i) = \mathbf{v}_i$ and $\dot{\mathbf{p}}(\mathbf{x}_i, \mathbf{p}_i) = \dot{\mathbf{p}}_i$, respectively, can be determined from the conditions $\mathbf{F}_i = 0$ and $\mathbf{T}_i = 0$, which state that the total force \mathbf{F}_i and torque \mathbf{T}_i on each microtubule are zero.

The forces and torques applied to microtubules are generated by the molecular motors that actively crosslink them. Here, motors are characterized by their force–velocity relation, the distance R (the motor size) over which they can crosslink filaments, and the crosslinking torque that they apply. The force that microtubule j exerts on microtubule i , via active crosslinks between $\mathbf{x}_i + s_i\mathbf{p}_i$ and $\mathbf{x}_j + s_j\mathbf{p}_j$ (Fig. 3a), is given by $\mathbf{F}_{ij}ds_i ds_j$ and the total force on microtubule i is

$$\mathbf{F}_i = \int_{-L/2}^{L/2} ds_i \sum_j \int_{-L/2}^{L/2} ds_j \int_{\Omega(\mathbf{x}_i + s_i\mathbf{p}_i)} d\mathbf{p}_j \int dx^3 \times \delta(\mathbf{x} - \mathbf{x}_j - s_j\mathbf{p}_j)\delta(\mathbf{p} - \mathbf{p}_j)\mathbf{F}_{ij} \quad (1)$$

where $\Omega(\mathbf{x})$ denotes a sphere of radius R centred at \mathbf{x} (Fig. 3b). The force density can be written as the divergence of the network stress tensor Σ according to Kirkwood’s formula since $\mathbf{F}_{ij} = -\mathbf{F}_{ji}$ (see Supplementary Information). The force balance of the network reads

$$\nabla \cdot \Sigma(\mathbf{x}) = \sum_i \mathbf{F}_i \delta(\mathbf{x} - \mathbf{x}_i) = \mathbf{0} \quad (2)$$

In a dense and highly crosslinked system, the motion of the fluid in which microtubules are suspended follows the microtubule motion and can be ignored (see Supplementary Information). The torque that crosslinkers between filaments i and j exert on filament i is given by $\mathbf{T}_{ij}ds_i ds_j$ with $\mathbf{T}_{ij} = s_i\mathbf{p}_i \times \mathbf{F}_{ij} + \Gamma_{ij}$, where Γ_{ij} is the contribution stemming from an explicit crosslinker torque. The total torque \mathbf{T}_i on microtubule i obeys an equation analogous to equation (1) (see Supplementary Information).

We model the XCTK2 motors by a force–velocity relation and a crosslinking torque density. The force density $\mathbf{F}_{ij}(\Delta\mathbf{v}_{ij})$ exerted by motors depends on the velocity difference $\Delta\mathbf{v}_{ij}$ between their two motor heads. The crosslinking torque density $\Gamma_{ij}(\mathbf{p}_i, \mathbf{p}_j)$ depends on their orientations. For simplicity, we ignore the effects of non-uniform distributions of motors along microtubules. Furthermore, we do not account for the buildup of elastic strain in the motors, which is a good approximation on timescales that are large compared to motor binding/unbinding times. To linear order in $\Delta\mathbf{v}_{ij}$

$$\mathbf{F}_{ij} = -\mathbf{G} \cdot \left[\mathbf{v}_i + s_i\dot{\mathbf{p}}_i + V\mathbf{p}_i - (\mathbf{v}_j + s_j\dot{\mathbf{p}}_j + V\mathbf{p}_j) \right] \quad (3)$$

where $V\mathbf{p}_i$ is the velocity of the motor relative to the microtubule it is bound to. This choice renders the force between two microtubules dependent on their relative polarities. The linear response coefficient \mathbf{G} is the motor friction and is in general a second rank tensor. In the following we choose $\mathbf{G} = \gamma\mathbf{I}$ for simplicity. Note that our results also hold for force velocity relations that are nonlinear in $\Delta\mathbf{v}_{ij}$ (see Supplementary Information). For the crosslinking torque

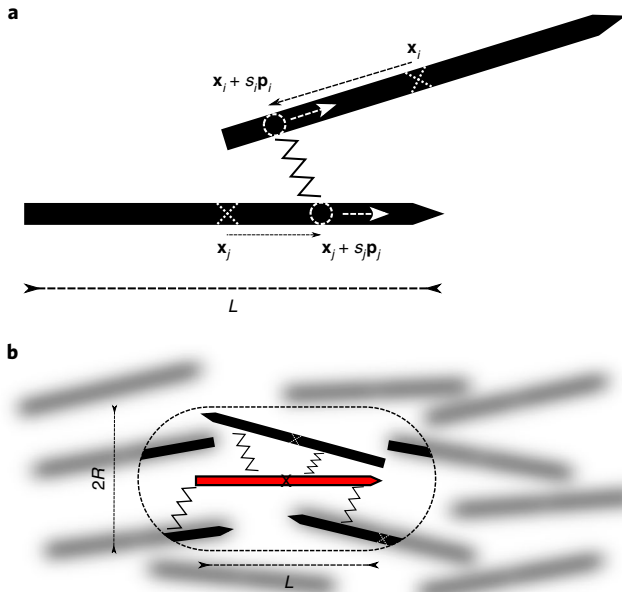


Fig. 3 | Sketch of the microscopic model. **a**, Each microtubule (black solid arrow) is characterized by its centre of mass position \mathbf{x} (white crosses) and its orientation \mathbf{p} . Microtubules interact via motor molecules (zigzag line), which connect them at arclength positions s_i, s_j (white circles) and walk towards their plus ends (white arrows). **b**, In the gel, crosslinkers of a test microtubule (red) explore all possible connections to other microtubules within reach (within the dashed capsule), that is, within a sphere of radius R around any position along the test microtubule.

density we choose $\mathbf{T}_{ij} = \nu \mathbf{p}_i \times \mathbf{p}_j (\mathbf{p}_i \cdot \mathbf{p}_j)$, which aligns microtubules, as would for example a torsional stiffness of the crosslinker. The coefficient ν characterizes the magnitude of this effect. Note that, dimensionally, \mathbf{F}_{ij} and \mathbf{T}_{ij} are forces and torques per area, respectively. It is straightforward to generalize our formulation to include motor activity that varies along the length of a filament, say by pausing at microtubule ends. This effect has been linked to network contractions^{20,27,35}.

We next derive a continuum theory for our system. We start by expanding equation (1) around the centre-of-mass positions \mathbf{x}_i and \mathbf{x}_j :

$$\begin{aligned} \mathbf{F}_i = & -\gamma L^2 \int_{\Omega(\mathbf{x}_i)} d\mathbf{x}^3 \rho(\mathbf{x}) [(\mathbf{v}_i - \mathbf{v}(\mathbf{x})) + V(\mathbf{p}_i - \mathbf{P}(\mathbf{x}))] \\ & -\gamma \frac{L^4}{12} \int_{\Omega(\mathbf{x}_i)} d\mathbf{x}^3 \nabla \cdot [\rho(\mathbf{x}) (\mathbf{p}_i \dot{\mathbf{p}}_i + \mathcal{H}(\mathbf{x}))] \end{aligned} \quad (4)$$

Here we have assumed that the length scale a of gradients in the system is large compared to the microtubule length L and dropped terms with more than two spatial derivative (see Supplementary Information). We also introduced density $\rho(\mathbf{x}) = \int d\mathbf{p} \psi(\mathbf{x}, \mathbf{p})$, the polarity $\mathbf{P}(\mathbf{x}) = \langle \mathbf{p}_i \rangle$, the rotation rate tensor $\mathcal{H}(\mathbf{x}) = \langle \mathbf{p}_i \dot{\mathbf{p}}_i \rangle$ and the velocity field $\mathbf{v}(\mathbf{x}) = \langle \mathbf{v}_i \rangle$, where the angled brackets $\langle \dots \rangle = 1/\rho \sum_i \int d\mathbf{p} \delta(\mathbf{x} - \mathbf{x}_i) \delta(\mathbf{p} - \mathbf{p}_i) \dots$ denote local averaging. The force balance equation (2) becomes

$$\begin{aligned} \nabla \cdot \boldsymbol{\Sigma}(\mathbf{x}) = & -\gamma L^2 \int_{\Omega(\mathbf{x})} d\mathbf{y}^3 \rho(\mathbf{x}) \rho(\mathbf{y}) \{ \mathbf{v}(\mathbf{y}) - \mathbf{v}(\mathbf{x}) + V(\mathbf{P}(\mathbf{y}) - \mathbf{P}(\mathbf{x})) \} \\ & -\gamma \frac{L^4}{12} \int_{\Omega(\mathbf{x})} d\mathbf{y}^3 \rho(\mathbf{x}) (\nabla \cdot (\rho(\mathbf{y}) \mathcal{H}(\mathbf{y})) + (\nabla \rho(\mathbf{y})) \cdot \mathcal{H}(\mathbf{x})) \end{aligned} \quad (5)$$

Now, using $R/a \ll 1$, we expand the integrand in equation (5) around \mathbf{x} and perform the integration. In this way, for the gel stress tensor we obtain

$$\boldsymbol{\Sigma} = \eta \rho^2 (\nabla \mathbf{v} + V \nabla \mathbf{P}) - \alpha \rho^2 \mathcal{H} \quad (6)$$

The coefficients $\eta = \gamma \frac{4\pi}{15} L^2 R^5$ and $\alpha = \gamma \frac{4\pi}{36} L^4 R^3$ have dimensions of viscosity by density squared. The first term of the stress tensor in equation (6) is viscous-like (that is, it depends on $\nabla \mathbf{v}$) and captures long-ranged coupling between microtubules. In contrast to a dilute suspension theory, in which a viscous coupling would be induced by the fluid, here it is induced by the crosslinkers. For active crosslinkers ($V \neq 0$) the stress-free state is self-straining and the gel's spontaneous strain rate is $\nabla \mathbf{v} = -V \nabla \mathbf{P}$. The second term of equation (6) is generated by microtubules reorienting in the gel and is analogous to a nematic alignment stress in liquid crystal theory. (We note that the ordering stress recovers the form derived for kinetic theories that approximate microtubule alignment by the Maier-Saupe free-energy²⁶ when using equation (8).) From equation (4), using $\nabla \cdot \boldsymbol{\Sigma} = 0$, we obtain the translational flux of microtubules:

$$\mathbf{v}_i - \mathbf{v} = -V(\mathbf{p}_i - \mathbf{P}) - \frac{L^2}{12} \frac{\nabla \rho}{\rho} \cdot (\mathbf{p}_i \dot{\mathbf{p}}_i - \mathcal{H}) \quad (7)$$

An analogous calculation for the torque balance (see Supplementary Information) yields

$$\alpha \mathbf{p}_i \times \dot{\mathbf{p}}_i = \hat{\nu} \mathbf{p}_i \times (\mathbf{p}_i \cdot \mathcal{Q}) \quad (8)$$

which is reminiscent of Maier-Saupe theory, where $\hat{\nu} = \nu L^2 \frac{4\pi R^3}{3}$ and where $\mathcal{Q}(\mathbf{x}) = \langle \mathbf{p}_i \mathbf{p}_i \rangle$ is the nematic tensor order parameter. The force balance $\nabla \cdot \boldsymbol{\Sigma} = 0$ and equations (6), (7) and (8) fully specify the system's dynamics and can be used to evolve the distribution of microtubule positions and orientations.

Comparison and interpretation

We next use the above described theory to investigate microtubule sliding in actively crosslinked networks. First we show that $\mathbf{v}_i = -V \mathbf{p}_i$ is the solution to an aligned network, which is the experimentally observed behaviour. Consider a fully aligned gel with all $\mathbf{p}_i = \pm \hat{\mathbf{e}}$, for some unit orientation vector $\hat{\mathbf{e}}$. With this, equation (8) yields $\dot{\mathbf{p}}_i = 0$. We make the ansatz $\mathbf{v}_i = -V \mathbf{p}_i + \mathbf{C}_0 + \mathbf{x}_i \times \mathbf{C}_1$, where $\mathbf{C}_0, \mathbf{C}_1$ denote constant rates of translation and rotation, respectively. After evaluating $\mathbf{v} = \langle \mathbf{v}_i \rangle$ and $\mathbf{P} = \langle \mathbf{p}_i \rangle$, this micro-scale ansatz obeys equation (7) and yields a macro-scale spatially uniform stress tensor satisfying $\boldsymbol{\Sigma} \equiv 0$. It thus solves the force balance $\nabla \cdot \boldsymbol{\Sigma} = 0$ with stress free boundary conditions for any system geometry. To determine the constants \mathbf{C}_0 and \mathbf{C}_1 we impose that the gel be at rest in the lab frame, such that $\sum_i \mathbf{v}_i = 0$ and $\sum_i \mathbf{x}_i \times \mathbf{v}_i = 0$, where we choose a coordinate system for which $\mathbf{x} = 0$ is the system's centre of mass. In our experiments, to good approximation $\sum_i \mathbf{p}_i = 0$ and $\sum_i \mathbf{x}_i \times \mathbf{p}_i = 0$, that is the total number of left and right pointing microtubules are approximately equal and polar domains are distributed homogeneously throughout the system. With this, we find $\mathbf{v}_i = -V \mathbf{p}_i$.

This means that all microtubules translate with the motor velocity in the direction of their plus end. The microtubule velocities are independent of the local polarity and only depend on the speed of the kinesin motors. This phenomenon is explained by motors generating an active strain rate in regions of varying polarity. Thus, microtubules can slide past each other without stressing the material because $\nabla \mathbf{v} = -V \nabla \mathbf{P}$; see equation (6). This surprising behaviour is a collective effect, as can easily be seen when considering the case of two isolated microtubules: two parallel microtubules linked by motors will be at rest in the lab frame, while two anti-parallel ones

will move. Ultimately, the system consists of two inter-penetrating gels of microtubules of opposite polarity that push against each other, with each gel held together by viscous coupling. In contrast, for sparsely crosslinked networks, the mass fluxes of left-moving and right-moving microtubules locally balance, leading to a strong dependence of sliding speed on the local polarity.

Thus our theory makes a series of quantitative predictions. First, the microtubules' sliding speed should be independent of the local network polarity. Second, the sliding velocity should be independent of the motor concentration. We find both of these predictions to be accurate in our experiments (Fig. 2). Third, we predict the sliding speed is set by the speed of the motor itself. We measured speeds of $18.6 \pm 0.9 \text{ nm s}^{-1}$, which are comparable to the single-molecule motor speeds of XCTK2 ($\sim 20 \text{ nm s}^{-1}$)³⁶. Importantly, our predictions do not depend on adjustable parameters and arise directly from the form of equations (1) and (3). In turn, the form of equation (3) results from imposing that molecular motors act uniformly along the length of the microtubules, which is a good approximation for the XCTK2 motor at high enough densities³⁶.

Polarity-independent sliding velocities are also observed in spindles formed in *Xenopus* egg extracts. These spindles consist of an array of microtubules that are anti-parallel near the spindle centre and highly polar at the spindle poles^{37,38}. Microtubules in these spindles continually slide toward spindle poles, a motion believed to be driven by the molecular motor kinesin-5¹¹. Due to the symmetries observed in spindles³⁸, $\sum_i \mathbf{v}_i \simeq 0$ and $\sum_i \mathbf{x}_i \times \mathbf{v}_i \simeq 0$, as in our in vitro

experiments. Because motors in spindles are abundant, we speculate that spindles might be self-straining, like the XCTK2–microtubule gel presented here. If this were the case, the speed of sliding should be the speed of kinesin-5 itself and constant throughout the spindle. Very suggestively, this is exactly what has been observed. In spindles, and particularly so when dynein is inhibited, microtubules slide at a constant speed^{12,13} that is approximately equal to the speed at which kinesin-5 slides apart pairs of anti-parallel microtubules in vitro³⁹. This suggests that, like our experimental system, spindles might consist of two inter-penetrating gels of microtubules of opposite polarity. Mechanically, this puts them in a regime between polymer suspensions and solid-like structures.

Our analytical framework can be used to investigate microtubule networks crosslinked by different motors. For example, dyneins pause and accumulate at microtubule minus ends⁴⁰. This motor dynamics can be implemented within our theory by modifying equation (3), which gives rise to \mathcal{Q} and ρ dependent active stresses (the calculation that predicts stresses for a generalized force–velocity curve will be presented in a subsequent publication). Such active stresses explain dynein-driven contractions of microtubule networks^{27,35,40}. Thus, the described theory generalizes previous models for network contractions²⁷ by providing a rigorous framework to predict how different motor properties give rise to different active stresses.

The self-straining state depends only on the balance between activity and viscous material response. Elastic deformations of either microtubules or motors do not play a role in this behaviour. Elastic, active networks can behave quite differently from the purely viscous systems^{31–33}. For example, in elastic, active polymer gels, passive crosslinkers facilitate the buildup of contractile stresses³⁴, which do not arise in the purely viscous limit. In our viscous theory, adding passive crosslinkers turns out to be exactly equivalent to slowing the motor. The interplay between viscous and elastic effects can be studied in our framework by augmenting equation (3) with elastic, history-dependent terms.

Many cytoskeletal networks are densely crosslinked. For example, the contractility of acto-myosin networks has been explained as emerging from its heavily crosslinked nature^{33,34}. The work presented here is an important step towards predicting the material

properties of actively crosslinked materials from the properties of their constituents and will enable the design of novel dynamics from first principles.

Reporting Summary. Further information on research design is available in the Nature Research Reporting Summary linked to this article.

Online content

Any methods, additional references, Nature Research reporting summaries, source data, statements of code and data availability and associated accession codes are available at <https://doi.org/10.1038/s41567-019-0642-1>.

Data availability

Figures 1 and 2 are based on microscopy data. The raw data are available from the authors upon reasonable request.

Received: 2 November 2018; Accepted: 17 July 2019;

Published online: 02 September 2019

References

- Marchetti, M. C. et al. Hydrodynamics of soft active matter. *Rev. Mod. Phys.* **85**, 1143–1189 (2013).
- Needleman, D. & Dogic, Z. Active matter at the interface between materials science and cell biology. *Nat. Rev. Mater.* **2**, 17048 (2017).
- Alberts, B. et al. *Molecular Biology of the Cell* 4th edn (Garland, 2002).
- Kruse, K., Joanny, J.-F., Jülicher, F., Prost, J. & Sekimoto, K. Generic theory of active polar gels: a paradigm for cytoskeletal dynamics. *Eur. Phys. J. E* **16**, 5–16 (2005).
- Joanny, J. F., Jülicher, F., Kruse, K. & Prost, J. Hydrodynamic theory for multi-component active polar gels. *New J. Phys.* **9**, 422 (2007).
- Jülicher, F., Grill, S. W. & Salbreux, G. Hydrodynamic theory of active matter. *Rep. Prog. Phys.* **81**, 076601 (2018).
- Bray, D. *Cell Movements: From Molecules to Motility* 2nd edn (Garland, 2001).
- Naganathan, S. R. et al. Morphogenetic degeneracies in the actomyosin cortex. *elife* **7**, e37677 (2018).
- Roostalu, J., Rickman, J., Thomas, C., Nédélec, F. & Surrey, T. Determinants of polar versus nematic organization in networks of dynamic microtubules and mitotic motors. *Cell* **175**, 796–808 (2018).
- Foster, P. J., Fürthauer, S., Shelley, M. J. & Needleman, D. J. From cytoskeletal assemblies to living materials. *Curr. Opin. Cell Biol.* **56**, 109–114 (2019).
- Mitchison, T. J. Mechanism and function of poleward flux in *Xenopus* extract meiotic spindles. *Phil. Trans. R. Soc. Lond. B* **360**, 623–629 (2005).
- Burbank, K. S., Mitchison, T. J. & Fisher, D. S. Slide-and-cluster models for spindle assembly. *Curr. Biol.* **17**, 1373–1383 (2007).
- Yang, G., Cameron, L. A., Maddox, P. S., Salmon, E. D. & Danuser, G. Regional variation of microtubule flux reveals microtubule organization in the metaphase meiotic spindle. *J. Cell Biol.* **182**, 631–639 (2008).
- Fürthauer, S., Stempel, M., Grill, S. W. & Jülicher, F. Active chiral fluids. *Eur. Phys. J. E* **35**, 1–13 (2012).
- Thampi, S. P., Golestanian, R. & Yeomans, J. M. Velocity correlations in an active nematic. *Phys. Rev. Lett.* **111**, 118101 (2013).
- Salbreux, G., Prost, J. & Joanny, J.-F. Hydrodynamics of cellular cortical flows and the formation of contractile rings. *Phys. Rev. Lett.* **103**, 058102 (2009).
- Mayer, M., Depken, M., Bois, J. S., Jülicher, F. & Grill, S. W. Anisotropies in cortical tension reveal the physical basis of polarizing cortical flows. *Nature* **467**, 617–621 (2010).
- Naganathan, S. R., Fürthauer, S., Nishikawa, M., Jülicher, F. & Grill, S. W. Active torque generation by the actomyosin cell cortex drives left–right symmetry breaking. *elife* **3**, e04165 (2014).
- Brugués, J. & Needleman, D. Physical basis of spindle self-organization. *Proc. Natl Acad. Sci. USA* **111**, 18496–18500 (2014).
- Kruse, K. & Jülicher, F. Actively contracting bundles of polar filaments. *Phys. Rev. Lett.* **85**, 1778–1781 (2000).
- Aranson, I. S. & Tsimring, L. S. Pattern formation of microtubules and motors: inelastic interaction of polar rods. *Phys. Rev. E* **71**, 050901 (2005).
- Liverpool, T. B. & Marchetti, M. C. Bridging the microscopic and the hydrodynamic in active filament solutions. *Europhys. Lett.* **69**, 846–852 (2005).
- Liverpool, T. B. & Marchetti, M. C. in *Cell Motility* (ed. Lenz, P.) 177–206 (Springer, 2008).
- Saintillan, D. & Shelley, M. J. Instabilities and pattern formation in active particle suspensions: kinetic theory and continuum simulations. *Phys. Rev. Lett.* **100**, 178103 (2008).

25. Saintillan, D. & Shelley, M. J. Instabilities, pattern formation and mixing in active suspensions. *Phys. Fluids* **20**, 123304 (2008).
26. Saintillan, D. & Shelley, M. J. Active suspensions and their nonlinear models. *C. R. Phys.* **14**, 497–517 (2013).
27. Foster, P. J., Fürthauer, S., Shelley, M. J. & Needleman, D. J. Active contraction of microtubule networks. *eLife* **4**, e10837 (2015).
28. Gao, T., Blackwell, R., Glaser, M. A., Betterton, M. D. & Shelley, M. J. Multiscale polar theory of microtubule and motor-protein assemblies. *Phys. Rev. Lett.* **114**, 048101 (2015).
29. Heidenreich, S., Dunkel, J., Klapp, S. H. L. & Bär, M. Hydrodynamic length-scale selection in microswimmer suspensions. *Phys. Rev. E* **94**, 020601 (2016).
30. Maryshev, I., Marenduzzo, D., Goryachev, A. B. & Morozov, A. Kinetic theory of pattern formation in mixtures of microtubules and molecular motors. *Phys. Rev. E* **97**, 022412 (2018).
31. Broedersz, C. P. & MacKintosh, F. C. Modeling semiflexible polymer networks. *Rev. Mod. Phys.* **86**, 995 (2014).
32. Ronceray, P. & Lenz, M. Connecting local active forces to macroscopic stress in elastic media. *Soft Matter* **11**, 1597–1605 (2015).
33. Ronceray, P., Broedersz, C. P. & Lenz, M. Fiber networks amplify active stress. *Proc. Natl Acad. Sci. USA* **113**, 2827–2832 (2016).
34. Belmonte, J. M., Leptin, M. & Nédélec, F. A theory that predicts behaviors of disordered cytoskeletal networks. *Mol. Syst. Biol.* **13**, 941 (2017).
35. Foster, P. J., Yan, W., Fürthauer, S., Shelley, M. J. & Needleman, D. J. Connecting macroscopic dynamics with microscopic properties in active microtubule network contraction. *New J. Phys.* **19**, 125011 (2017).
36. Hentrich, C. & Surrey, T. Microtubule organization by the antagonistic mitotic motors kinesin-5 and kinesin-14. *J. Cell Biol.* **189**, 465–480 (2010).
37. Yu, C.-H. et al. Measuring microtubule polarity in spindles with second-harmonic generation. *Biophys. J.* **106**, 1578–1587 (2014).
38. Brugués, J., Nuzzo, V., Mazur, E. & Needleman, D. J. Nucleation and transport organize microtubules in metaphase spindles. *Cell* **149**, 554–564 (2012).
39. Kapitein, L. C. et al. The bipolar mitotic kinesin Eg5 moves on both microtubules that it crosslinks. *Nature* **435**, 114–118 (2005).
40. Tan, R., Foster, P. J., Needleman, D. J. & McKenney, R. J. Cooperative accumulation of dynein–dynactin at microtubule minus-ends drives microtubule network reorganization. *Dev. Cell* **44**, 233–247 (2018).

Acknowledgements

C.E.W. acknowledges support by NIH R35GM122482. D.J.N. acknowledges the Kavli Institute for Bionano Science and Technology at Harvard University and National Science Foundation grants PHY-1305254, PHY-0847188, DMR-0820484 and DBI-0959721. P.J.F. acknowledges support from the Gordon and Betty Moore Foundation for support as a Physics of Living Systems Fellow through grant no. GBMF4513. M.J.S. acknowledges support from National Science Foundation grants DMR-0820341 (NYU MRSEC), DMS-1463962 and DMS-1620331. Z.D. acknowledges support from NSF MRSEC DMR-1420382.

Author contributions

S.F., M.J.S. and D.J.N. developed the theory. B.L., P.J.F., S.C.E.-M., C.-H.Y., C.E.W. and Z.D. performed experiments and provided materials. S.F., B.L., D.J.N. and M.J.S. wrote the paper with input from all authors.

Competing interests

The authors declare no competing interests.

Additional information

Supplementary information is available for this paper at <https://doi.org/10.1038/s41567-019-0642-1>.

Reprints and permissions information is available at www.nature.com/reprints.

Correspondence and requests for materials should be addressed to S.F.

Peer review information: *Nature Physics* thanks Karin John, Gijse Koenderink and the other, anonymous, reviewer(s) for their contribution to the peer review of this work.

Publisher's note: Springer Nature remains neutral with regard to jurisdictional claims in published maps and institutional affiliations.

© The Author(s), under exclusive licence to Springer Nature Limited 2019

Reporting Summary

Nature Research wishes to improve the reproducibility of the work that we publish. This form provides structure for consistency and transparency in reporting. For further information on Nature Research policies, see [Authors & Referees](#) and the [Editorial Policy Checklist](#).

Statistical parameters

When statistical analyses are reported, confirm that the following items are present in the relevant location (e.g. figure legend, table legend, main text, or Methods section).

n/a Confirmed

- The exact sample size (n) for each experimental group/condition, given as a discrete number and unit of measurement
- An indication of whether measurements were taken from distinct samples or whether the same sample was measured repeatedly
- The statistical test(s) used AND whether they are one- or two-sided
Only common tests should be described solely by name; describe more complex techniques in the Methods section.
- A description of all covariates tested
- A description of any assumptions or corrections, such as tests of normality and adjustment for multiple comparisons
- A full description of the statistics including central tendency (e.g. means) or other basic estimates (e.g. regression coefficient) AND variation (e.g. standard deviation) or associated estimates of uncertainty (e.g. confidence intervals)
- For null hypothesis testing, the test statistic (e.g. F , t , r) with confidence intervals, effect sizes, degrees of freedom and P value noted
Give P values as exact values whenever suitable.
- For Bayesian analysis, information on the choice of priors and Markov chain Monte Carlo settings
- For hierarchical and complex designs, identification of the appropriate level for tests and full reporting of outcomes
- Estimates of effect sizes (e.g. Cohen's d , Pearson's r), indicating how they were calculated
- Clearly defined error bars
State explicitly what error bars represent (e.g. SD, SE, CI)

Our web collection on [statistics for biologists](#) may be useful.

Software and code

Policy information about [availability of computer code](#)

Data collection

imageJ, uManager, Becker & Hickl GmbH acquisition software

Data analysis

imageJ, Matlab, GitHub for the code is provided in the Supplementary Materials.
https://github.com/bezlemma/2017_BleachPolarity_And_Velocity_Analysis

For manuscripts utilizing custom algorithms or software that are central to the research but not yet described in published literature, software must be made available to editors/reviewers upon request. We strongly encourage code deposition in a community repository (e.g. GitHub). See the Nature Research [guidelines for submitting code & software](#) for further information.

Data

Policy information about [availability of data](#)

All manuscripts must include a [data availability statement](#). This statement should provide the following information, where applicable:

- Accession codes, unique identifiers, or web links for publicly available datasets
- A list of figures that have associated raw data
- A description of any restrictions on data availability

The microscopy data that support the findings of this study are available from Bezia Lemma upon reasonable request.

Field-specific reporting

Please select the best fit for your research. If you are not sure, read the appropriate sections before making your selection.

Life sciences Behavioural & social sciences Ecological, evolutionary & environmental sciences

For a reference copy of the document with all sections, see [nature.com/authors/policies/ReportingSummary-flat.pdf](https://www.nature.com/authors/policies/ReportingSummary-flat.pdf)

Life sciences study design

All studies must disclose on these points even when the disclosure is negative.

Sample size	For a given set of experimental conditions, bleaching behavior was measured at >20 different locations.
Data exclusions	No data was excluded.
Replication	Results were successfully reproduced in different realizations.
Randomization	There is no intentional randomization in these studies.
Blinding	Not relevant for our studies.

Reporting for specific materials, systems and methods

Materials & experimental systems

n/a	Included in the study
<input type="checkbox"/>	<input checked="" type="checkbox"/> Unique biological materials
<input checked="" type="checkbox"/>	<input type="checkbox"/> Antibodies
<input checked="" type="checkbox"/>	<input type="checkbox"/> Eukaryotic cell lines
<input checked="" type="checkbox"/>	<input type="checkbox"/> Palaeontology
<input checked="" type="checkbox"/>	<input type="checkbox"/> Animals and other organisms
<input checked="" type="checkbox"/>	<input type="checkbox"/> Human research participants

Methods

n/a	Included in the study
<input checked="" type="checkbox"/>	<input type="checkbox"/> ChIP-seq
<input checked="" type="checkbox"/>	<input type="checkbox"/> Flow cytometry
<input checked="" type="checkbox"/>	<input type="checkbox"/> MRI-based neuroimaging

Unique biological materials

Policy information about [availability of materials](#)

Obtaining unique materials	Plasmids for the labeled and unlabeled XCTK2 is available upon request.
----------------------------	---